Sensors & Transducers, Vol. 231, Issue 3, March 2019, pp. 15-24

www.sensorsportal.com

Sensors & Transducers

Published by IFSA Publishing, S. L., 2019
http://www.sensorsportal.com

Modelling and Simulation of Various Kinds of Blockage in Carotid Artery and Finding Their Pressure and Velocity Gradient Suitable for Measuring These Parameters Noninvasively with the Help of External Pressure and Velocity Sensors

*** Kshitij SHAKYA and Shubhajit ROY CHOWDHURY**
School of Computing and Electrical Engineering
IIT Mandi, Kamand-175005, Mandi, H. P., India
* Tel.: +91 1905 267110, fax: +91 1905 267009
E-mail: src@iitmandi.ac.in

Received: 30 January 2019 /Accepted: 5 March 2019 /Published: 29 March 2019

Abstract: This paper considers the blood flow in carotid artery and its adjoining internal and external carotid artery. It focuses on different shapes of obstructions developed in the artery due to plaque formation by fat and cholesterol deposit. The current research takes into consideration the specific areas of plaque formation and the overall consequence on pressure and velocity distribution accordingly throughout the artery. This simulation gives the pressure and velocity profiles at different points which may be measured non-invasively by MEMS pressure sensor and Doppler velocimeter externally. The study made in this paper is also useful in locating the probable area of blockage and the shape of blockage. The simulation also studies thickening of blood and the effect of external pressure application on the artery. The simulation has been carried out using Comsol Multiphysics 5.3 where a 3d model of carotid artery adjoining internal and external carotid artery along with blockages has been taken into consideration. This study assumes that the fluid is Newtonian, non-viscous and incompressible. Fluid flow is laminar and the arterial wall is elastic.

Keywords: COMSOL multiphysics; Blood vessel; Spherical, hemispherical and Gaussian shaped blockages; Carotid artery disease, Vascular resistance

1. Introduction

Atherosclerosis majorly contributes to the cause of death and premature disability in developing and developed countries. The current predictions estimates that by 2020 cardiovascular diseases, mainly atherosclerosis will become the leading global cause of total diseases. The Blockage in the arteries supplying blood to brain causes strokes and cerebral ischemia [1].

The most cases of carotid artery stenosis are caused by atherosclerotic plaque as part of generalized atherosclerotic disease. Carotid Artery Stenting (CAS) has been initially used as an alternative treatment option in patients not eligible for surgery [2]. It is hard to reconcile the modest number of patients who are at increased 10-year risk by the Framingham CV risk model with the observation that the lifetime risk of Coronary Artery Disease (CAD) starting at age 40 years is 49 % for

men and 32 % for women [3]. Carotid plaque is associated with traditional and non-traditional CV risk factors. Several studies have shown that carotid plaque, either alone or combined with other screening tests and information from the patient's history, predicts the presence of cardiac ischemia and angiographic CAD [2].

The early lesions in the tunica intima (innermost layer of artery) arise from increase in accumulation of lipoproteins within the regions of tunica intima. Lipoprotein particles may undergo oxidative modifications in the extracellular space of intima. Leukocyte Accumulation also characterizes the formation of atherosclerotic lesions. Leukocyte adhesion can be decreases by laminar shear forces in most regions of normal arteries [4]. Favourable sites for atherosclerotic lesions e.g. Branch points often have disturbed flow. Pulsatile and ordered laminar shear of normal blood flow increases the production of nitric acid by endothelial cells. The endothelial cells having properties which dilates the blood vessels limits the adhesion of lipoproteins. Production of superoxide dimulatse by stimulation endothelial cells is also caused by laminar shear stress, an antioxidant enzyme [1]. These examples explain the favoured sites of atherosclerotic lesions due to disturbance in laminar shear stress.

The monocytes and lymphocytes penetrate the endothelial layer when captured on the surface of the arterial endothelial cells by receptors and take up residence in the intima. After that, the mononuclear phagocytes forms into macrophages and lipid laden foam cells is resulted. Thus key steps in formation of atherosclerotic plaques are firstly, monocyte attachment to endothelium secondly, migration into the intima and thirdly maturation to form lipid-laden macrophages [1].

Major risk factors for developing atherosclerotic plaque includes Cigarette smoking, blood pressure above 140/90 mmHg, low HDL cholesterol, high LDL cholesterol, fasting triglycerides >150 mg/dl, Diabetes mellitus, obesity, physical inactivity, atherogenic diet etc. [1, 14, 16].

This paper considers a 3D model of a part of carotid artery with a branch which is the favorable site for plaque deposition. Three types of blockage has been discussed in this paper, hemisphere and Gaussian shaped blockages indicating to be developed from adhesion of leukocytes resulting in atherosclerotic plaques and sphere shaped blockage as result of embolus has been considered. Firstly the velocity and pressure profile throughout the healthy artery is presented then the same has been calculated for different shapes of all the three types of blockages. Next, the results for stiffening of the artery, vascular resistance, thickening of blood and the effect of external pressure application on the artery have also been calculated. A simulation study of detection of blockage and its extent by assuming two pairs of external pressure sensors along carotid has also been discussed.

The aim of this paper is to compare the scenarios between a healthy artery and the artery with disease describing the changes in the blood flow, plaque formation, blood flow velocity and pressure. This computer simulated model is helpful in analyzing the possibility of occurrence of CAD and learning the behaviour and consequences of the plaque getting deposited regularly. The model also simulates the formation and growth of the plaque and observes the changes in blood flow which is faster, simpler and safer before doing the treatment.

This paper is organized as follows: Section 2nd shows the modelling of carotid artery and types of blockages. Section 3rd discusses the results regarding the pressure and velocity distribution. Section 4th concluded the paper and briefs about future perspectives.

2. Modelling of Carotid Artery

The common carotid artery along with its adjacent branch of internal and external carotid artery is modelled as shown in Fig. 1. The approximate length of common, external and internal carotid artery is 50 mm, 40 mm and 30 mm and internal diameter of 6 mm, 5 mm and 4 mm respectively. Three different types of blockages has been modelled. The Gaussian shaped and hemisphere shaped at the branch points and sphere shaped at a point at plain lumen surface. The blockages are shown as to be increased with time with a definite increase in the thickness of the blockage. To model blood flow the laminar flow of fluid mechanics and to study the pressure due to it the solid mechanics physics has been used accompanied by stationary solver. The blood fluid material is assumed to be Newtonian here because the apparent viscosity of blood is almost constant due to high shear rates [8, 11], 13]. Also it is assumed to be non-viscous, incompressible and artery walls have been assumed to be elastic. The blood flow is governed by the continuity equation and Navier-Stokes [5, 10, 18], equation.

Fig. 1 shows the common carotid artery with its distributed internal and external carotid arteries. The bottom of the artery is the inlet for the blood flow. Fig. 2 on the other hand shows the same but with two outlets corresponding to the inlet.

Blood flow through a blood vessel is determined by pressure difference of the blood between the two ends of the vessel, also called pressure gradient along the vessel, which is the force that pushes the blood through the vessel, and the impediment to blood flow through the vessel, which is called vascular resistance [17]. P1 represents the pressure at the origin of the vessel; at the other end, the pressure is P2. Resistance is resulted because of friction between the flowing blood and the intravascular endothelium layer of the vessel. The flow through the vessel can be calculated by the Ohm's law: in which Q is blood flow, ΔP is

the pressure difference between the two ends of the vessel, and R is the resistance [7, 12, 16]:

$$Q = \frac{\Delta P}{R} \tag{1}$$

This formula states, in effect, that the blood flow is directly proportional to the pressure difference but inversely proportional to the resistance.

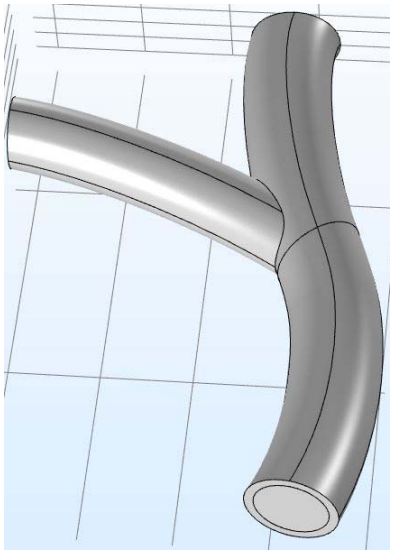

Fig. 1. Carotid artery with two distributed branches.

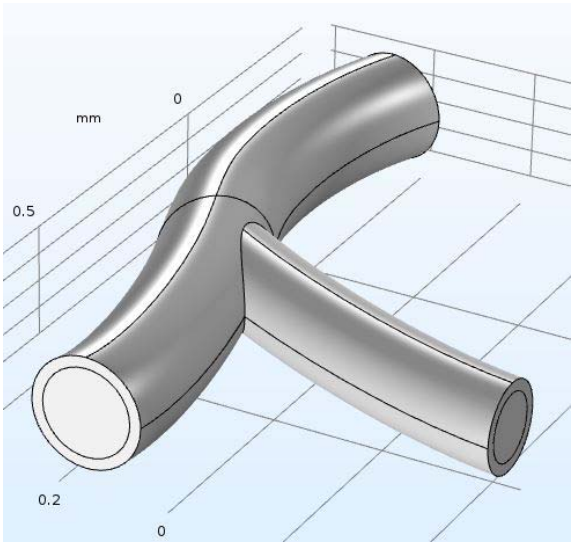

Fig. 2. Carotid artery (Front view).

2.1. Calculation of Pressure over Carotid Artery

Considering a cylinder representing the artery having a Gaussian shaped blockage and two MEMS pressure sensor capable to sense the arterial wall pressure due to blood flow. One of them is fixed at the origin of cylinder and treated as reference pressure sensor and other is movable. P1 is the point at which fixed sensor is placed. P2 is the point at which the height of blockage is maximum and P3 is the point further away from P2. The area of blockage can be assumed as sector due to small dimensions.

The above Fig. 3 shows the cross section view of the blockage indicating that as the size increases the area of the sector increases and hence the θ also increases.

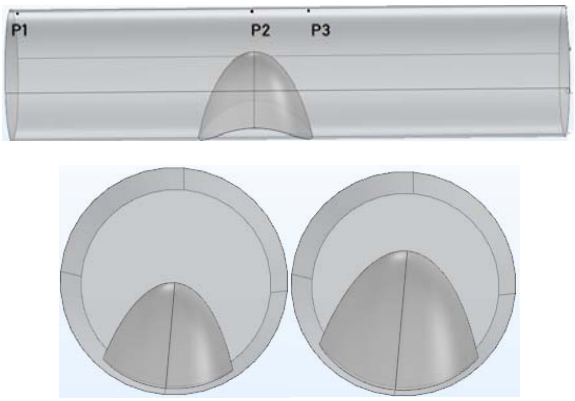

Fig. 3. Horizontal and cross-section view of assumed cylinder.

Area of cross section at P1, $A1 = \frac{\pi d_1^2}{4}$.

Area of cross section at P2 excluding the area of sector

$$A2 = \frac{\pi d_1^2}{4} - \frac{\pi d_1^2}{4} \times \frac{\theta}{360}$$
$$A2 = \frac{\pi d_1^2}{4}\left(1 - \frac{\theta}{360}\right) \tag{2}$$

or

$$\frac{A2}{A1} = 1 - \frac{\theta}{360}$$

By equation of continuity

$$A1\ v1 = A2\ v2$$

or

$$\frac{A2}{A1} = \frac{v1}{v2} = 1 - \frac{\theta}{360} \tag{3}$$

From Bernoulli's theorem

$$gh + \frac{v^2}{2} + \frac{p}{\rho} = constant$$

Since the cylinder is horizontal we can neglect height, h

$$\frac{v_1^2}{2}+\frac{p1}{\rho}=\frac{v_2^2}{2}+\frac{p2}{\rho}$$

or

$$p1-p2=\rho\left(\frac{v_2^2-v_1^2}{2}\right) \quad (4)$$

Putting value of Eq. (3) in Eq. (4)

$$\Delta p=\frac{\rho v_2^2}{2}\left(\frac{720\theta-\theta^2}{360^2}\right), \quad (5)$$

where v_1 and p1 are the velocity and pressure at point P1, v_2 and p2 are the velocity and pressure at point P2, Δp is change in pressure at point P1 and P2 and ρ is the density of blood. This value of Δp can be used to detect the blockage and size of blockage as shown in further sections.

2.2. Calculation of Velocity over Carotid Artery

Considering the same cylinder as shown in Fig. 3. For measuring velocity two ultrasonic sensors can be placed over the artery. The velocity of blood can be calculated using transit time difference and Doppler frequency shift. The relation between transit time difference and blood flow velocity can be calculated as

$$\Delta t=\frac{2Dv\cos\alpha}{c^2} \quad (6)$$

And the relation between Doppler frequency shift and blood flow velocity can be calculated as

$$\Delta f=\frac{2fv\cos\alpha}{c}, \quad (7)$$

where c is the speed of ultrasonic waves, D is the artery diameter and α is the angle at which ultrasonic waves are incident. The blockage can be easily detected by detecting the change in velocity going throughout the length of the artery.

The model contains three domains, one forms the cylinder containing the walls of the artery, second forms the space where blood flows and the third is for the fat or cholesterol structure forming the plaque (Table 1).

Table 1. Material properties [5].

Properties	Blood	Artery	Fat deposit
Density (Kg/m^3)	1060	1060	1050
Dynamic Viscosity (Pa.s)	0.005	-	-
Young's modulas (MPa)	-	2	20
Poisson's ratio	-	0.49	0.11

The flow under laminar flow physics was modelled for blood as Newtonian fluid with no slip boundary condition. Two boundaries for inlet and outlet flow have been selected with inlet velocity of 0.169 m/s and outlet pressure of 0 atm.

The Gaussian, hemispherical and spherical blockages contained by the arterial lumen are shown in Fig. 4, Fig. 5 and Fig. 6.

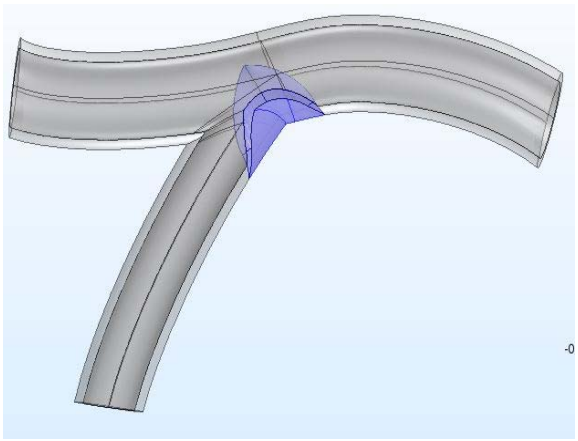

Fig. 4. Artery with Gaussian blockage.

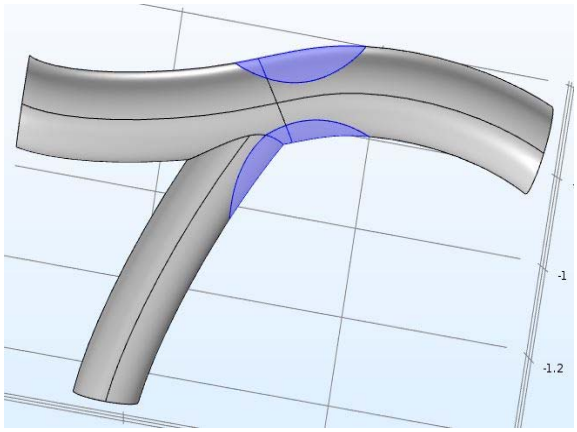

Fig. 5. Artery with hemispherical blockage.

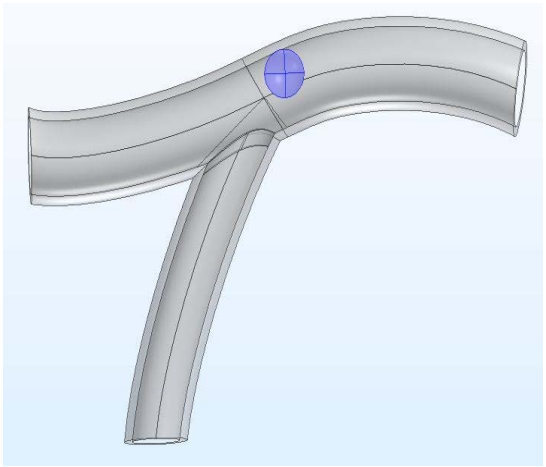

Fig. 6. Artery with spherical blockage.

Fig. 6 shows the points drawn throughout the geometry to take a record of pressure and velocity at those points. Two points are drawn across the blockage site on the arterial wall and the corresponding two points are drawn just below them in the middle of the artery. Two such points are also drawn on the artery with smaller cross section area. And these are the points where sensors can be placed externally to verify the following results.

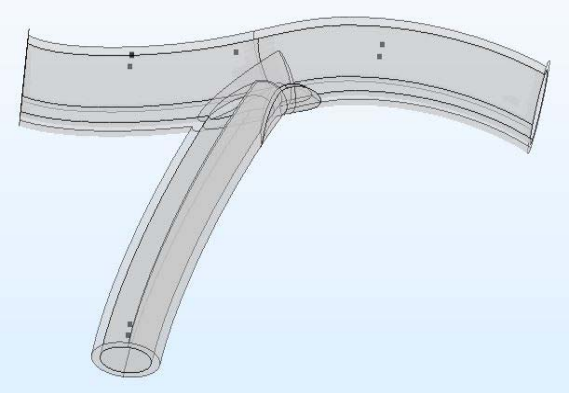

Fig. 6. Position for placing sensors.

3. Results and Discussion

The analytical work in Eq. (5) can be validated using Comsol. It has been shown in this section that how closely both the calculation of pressure difference and its measurement by Comsol vary. Putting the value of density of blood in Eq. (5) it becomes

$$\Delta p = 530 v_2^2 \left(\frac{720\theta - \theta^2}{360^2} \right) \quad (8)$$

It can be seen that as the obstruction increases at point P2, the area for fluid flow becomes less, increasing the velocity at P2 and it is evident from Bernoulli's equation that due to increment in velocity the pressure at P2 decreases. Hence Δp (p1-p2) goes on increasing as blockage increases. Hence the movable pressure sensor can be kept at different points throughout the artery and the point of maximum pressure difference (Δp) can be concluded as the site for blockage/maximum blockage.

Calculating Δp by putting different values of θ, indicating the increase in blockage size Table 2 has been plotted for θ= 30, 60, 90, 120 and 150 degrees.

Table 2. Relation between θ and Δp according to Eq. (5).

θ	Δp
30	$84.65v^2$
60	$161.94v^2$
90	$231.87v^2$
120	$294.44v^2$
150	$349.65v^2$

Also velocities measured from Eq. (6) and Eq. (7) can be put in Table 2 to get the change in pressure for every size of blockage and hence can be verified from the values of MEMS pressure sensors.

Next, to validate the results shown in Eq. (8) and Eq. (6), the geometry shown in Fig. 3 has been simulated in Comsol and the velocities and pressure at points P1 and P2 has been shown in Table 3 and Table 4.

Table 3. Velocities at P1 and P2 at different values of θ.

Velocity (m/s) at P1	Velocity (m/s) at P2	θ
0.160	0.172	30
0.173	0.198	60
0.164	0.266	90
0.154	0.291	120
0.174	0.322	150

As calculated earlier using Bernoulli's theorem, the pressure at point is less since the velocity at that point increases in every case. Next the plot for Δp from Table 4 which is calculated by Comsol and the plot for Δp from Table 2, found analytically by putting the values of v at point P2 from Table 3 has been plotted in Fig. 7.

Table 4. Pressure at P1 and P2 at different values of θ.

Pressure (Pa) at P1	Pressure (Pa) at P2	θ	Δp
24.99	12.92	30	12.07
41.98	22.67	60	19.31
78.49	46.06	90	32.43
138.89	93.56	120	45.33
180.55	188.06	150	62.49

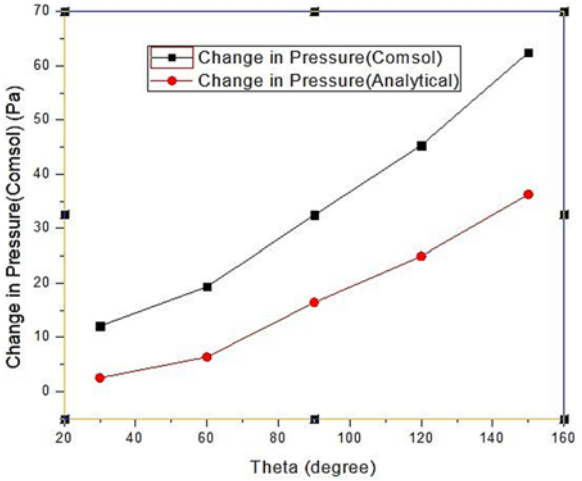

Fig. 7. Change in pressure for both cases.

The plot in Fig. 7 shows proportional increase of both the pressures changes and differs by some constant factor. Hence it is evident from this figure that this Δp can be used to detect the blockage

and its growth and can be treated well before its dangerous consequences.

The pressure and velocity profile of the healthy artery has been plotted and shown in Fig. 8 and Fig. 9. The colour pattern of Comsol results indicates red, orange yellow green, violet blue with red being the highest and blue lowest value. As intuitive the pressure is maximum from the inlet and then decreases to the outlets. The internal carotid branch of the artery shows less velocity and pressure due to its small cross sectional area as compared to common carotid artery.

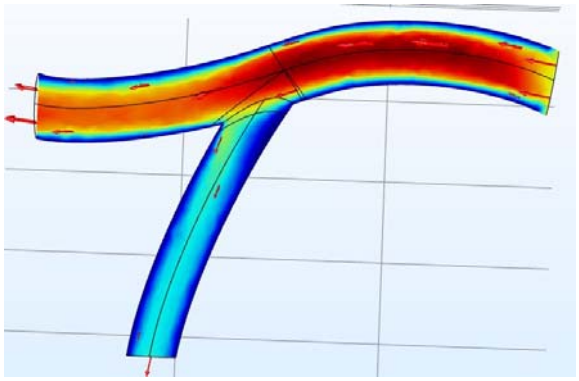

Fig. 8. Velocity profile of a healthy artery.

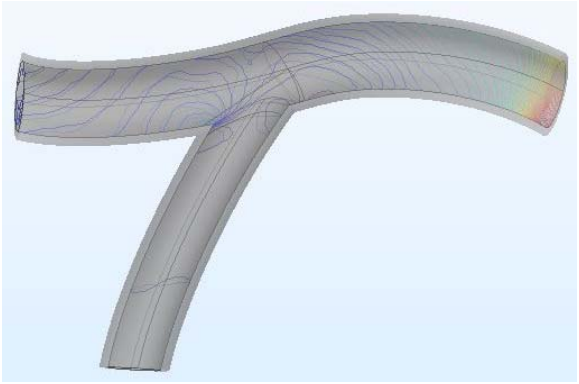

Fig. 9. Pressure profile of healthy artery.

Table 5. Pressure and velocity at points across the blockage site in case of healthy artery.

	Point 1	**Point 2**
Pressure (Pa) At mid artery region	7.243	4.34
Pressure (Pa) At arterial wall region	7.470	4.602
Velocity (m/s) At mid artery region	0.253	0.185
Velocity (m/s) At arterial wall region	0.044	0.029

The considerable difference at both points in the parameters even without the blockage is due to the distribution of blood in two branches of the artery.

Next, the geometry with Gaussian curved blockage has been simulated. The fat geometry has been inserted in the artery with succession of 0.02 mm until it closes most of the artery. The velocity profiles with initial and final shape of Gaussian blockage are shown in Fig. 10 and Fig. 11.

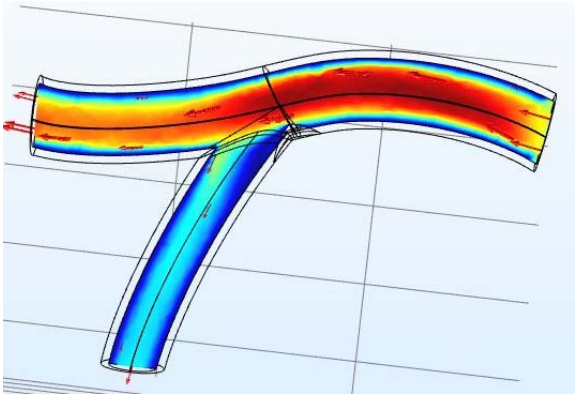

Fig. 10. Velocity profile of initial Gaussian blockage.

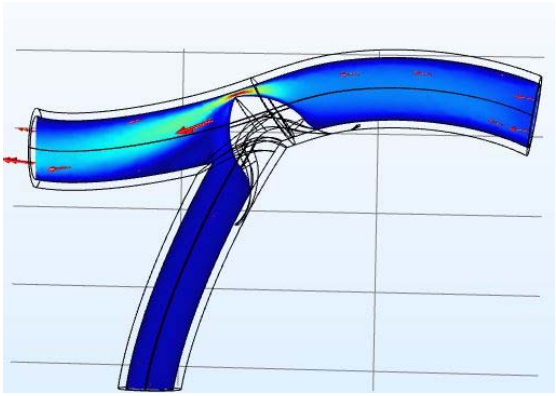

Fig. 11. Velocity profile when the size of Gaussian blockage is maximum.

The pressure at post blockage site (point 2) and the pressure in internal carotid artery as the Gaussian blockage starts increasing is plotted Fig. 12.

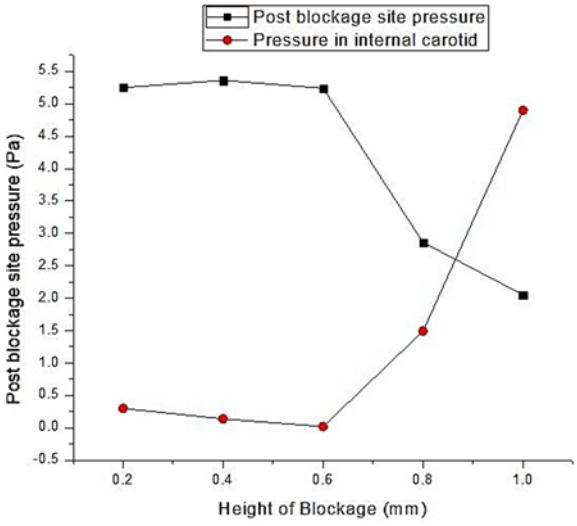

Fig. 12. Pressure at post blockage site and internal carotid against increasing Gaussian blockage.

Fig. 13 displays the pre blockage site (point 1) pressure against varying increase in Gaussian blockage.

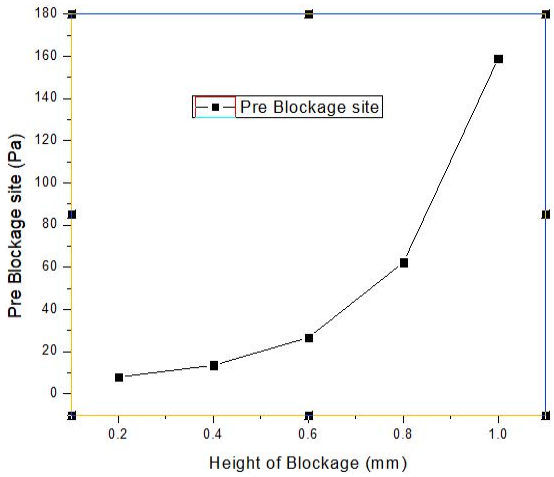

Fig. 13. Pressure at pre blockage site against increasing Gaussian blockage.

The plot in Fig. 11 shows an interesting pattern of blood flow along main artery and the internal carotid artery. Up to 0.8 mm blockage both graphs look like a mirror image. Up to 6 mm blockage the pressure decrement at post blockage site is compensated by the increment in internal carotid artery. This is due to the fact that since the blood flow is constant the increased blood flow in former case is compensated by the decreased blood flow in latter. From 0.6 mm to 1 mm there is an abrupt decrease at post blockage site and a corresponding increase in pressure in internal carotid. The plot also reveals that the pressure at these to point comes to same at 0.88 mm blockage height. This kind of pattern can be thought as a finger print pattern for the given shape of artery and blockage. If the pressure is measured at these locations externally then getting these pattern of pressure profile can confirm the Gaussian shape of the blockage present at the artery. Fig. 11 shows the steady exponential increase in pressure because the pre blockage site faces all the blood interaction there is no distributed artery to make any variation.

The Fig. 14 shows the velocity profile for the points located at internal carotid artery and at post blockage site which when comparing to Fig. 11 justifies the increment and decrement well up to 0.8 mm blockage.

The same analysis has been for a hemisphere shaped blockage. The blockage geometry was increased in succession till it completely clogged the artery and then their corresponding velocity and pressure profile were measured at specific points. Fig. 15 shows the pressure profile at post blockage site and pressure at internal carotid against an increase in height of hemispherical blockages until both the hemisphere arcs touches each other. The graph shows the pattern like previous case that the decrement in pressure at post blockage site is compensated by increase in pressure at internal carotid, because the distributed flow of blood in both the branches. The blood flow being constant the increase of blood flow in one branch decreases the flow in other. Fig. 14 on the shows the pressure at pre blockage site which like the previous blockage shows increase at every interval. This kind of pattern can also be treated as fingerprint flow pattern of the artery with hemispherical blockage.

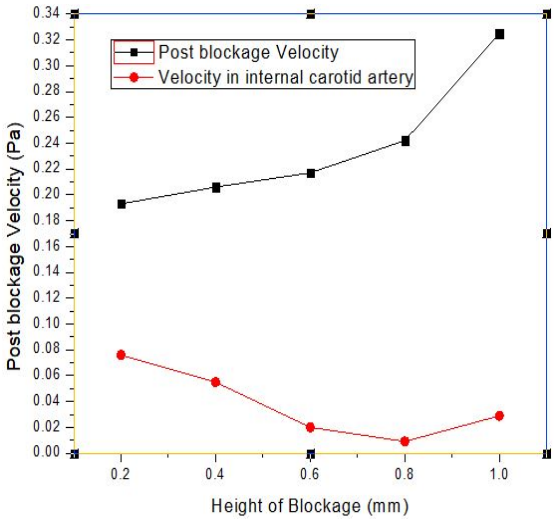

Fig. 14. Velocity profile for internal carotid artery and the point and post blockage.

The velocity profile for both post blockage site and internal carotid artery is plotted in Fig. 17.

The scenario here is different as from the previous cases because from 0.4 to 0.8 mm blockage the velocity increases for both the cases.

Next the pressure profile for spherical blockages has been discussed. Fig. 18 shows the relation between size of the spherical blockage and pressure at post blockage site and pressure at a point inside internal carotid artery.

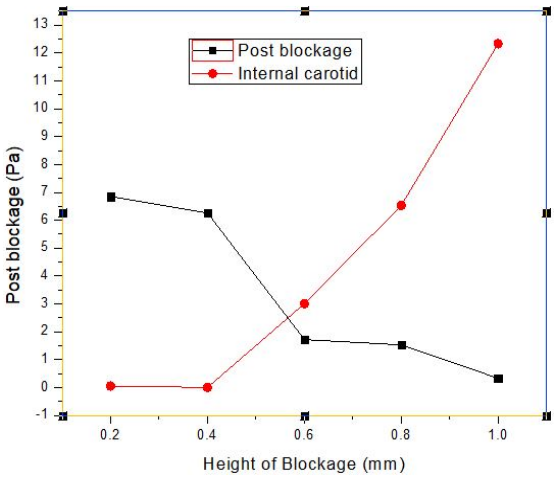

Fig. 15. Pressure profile for hemispherical blockage at post blockage site and internal carotid.

The post blockage site pressure continue to decrease as the blockage is hindering the blood flow and the pressure in internal carotid branch remains almost same and then decreases for a bit since the blockage doesn't hinder the flow in it much. The velocity profile for the same is also plotted and shown in Fig. 19.

The velocity at the post blockage site decreases just like the decrease in pressure and the velocity in carotid artery also follow the pressure in it as shown in Fig. 16. Fig. 17 also shows that both the graphs are almost a mirror image implying that the decrease in velocity in one branch is an increment in the other since due to the blockage the fluid is diverted to the other branch more.

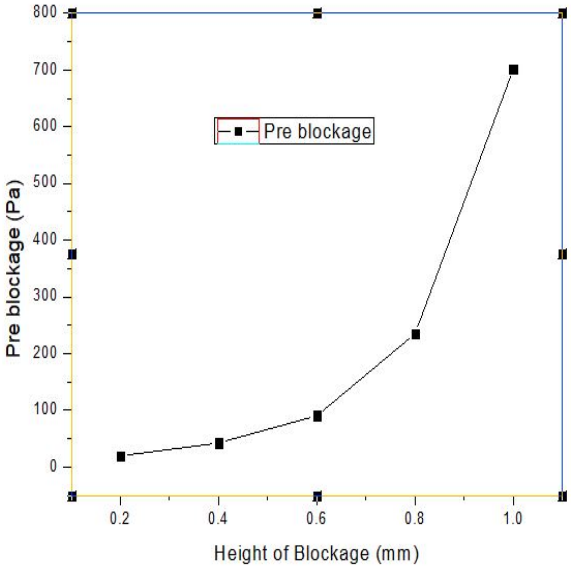

Fig. 16. Pre blockage pressure in case of hemispherical blockages.

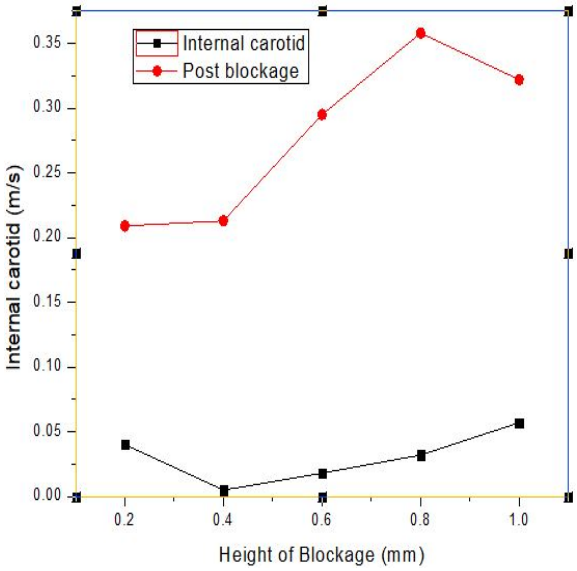

Fig. 17. Velocity profile at internal carotid and post blockage site.

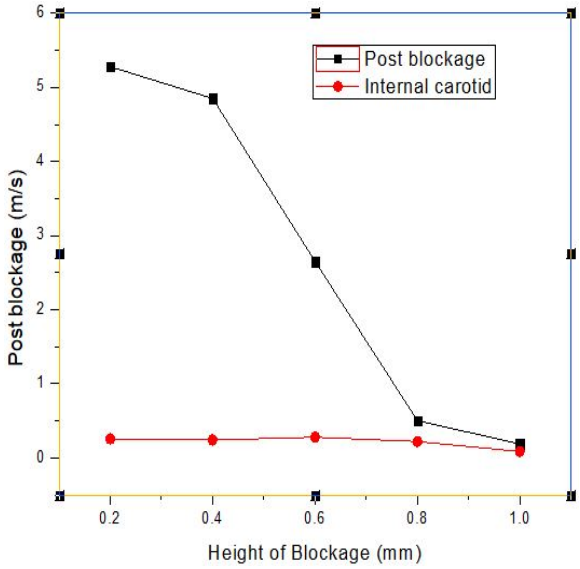

Fig. 18. Pressure at post blockage site and internal carotid artery in case of spherical blockages.

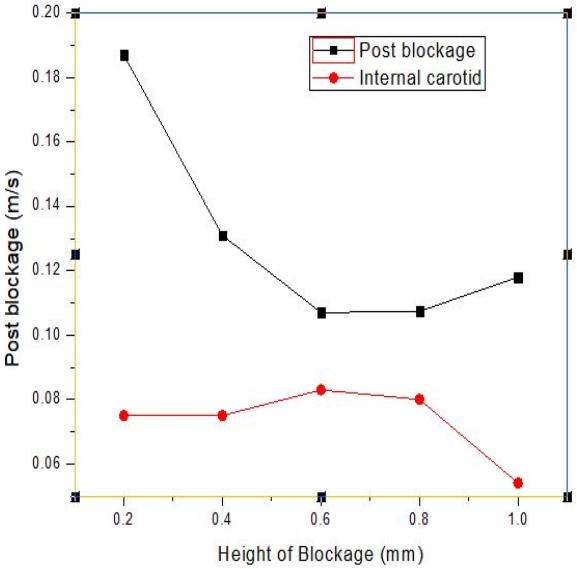

Fig. 19. Velocity at post blockage site and internal carotid artery in case of spherical blockages.

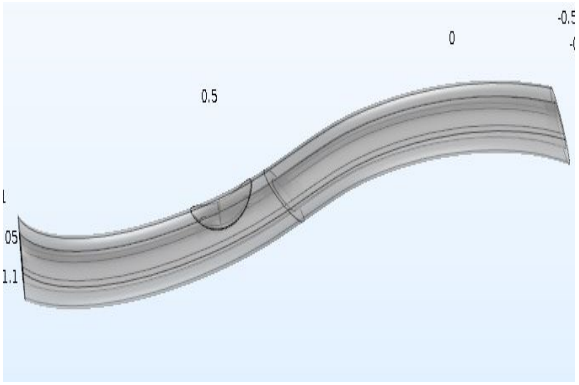

Fig. 20. Geometry only for common carotid artery.

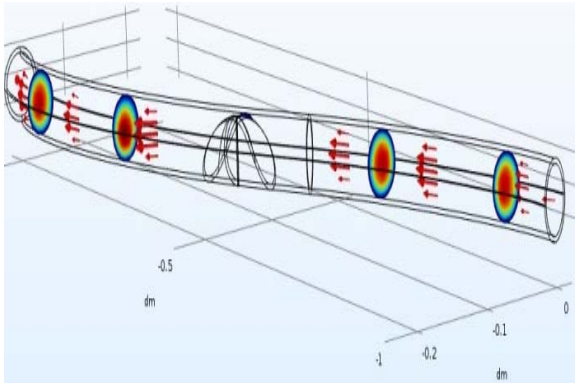

Fig. 21. Velocity profile with geometry with only carotid artery.

Next, the geometry for only common carotid artery has been considered. This geometry doesn't contain any branch of internal carotid artery like the previous case and is shown in Fig. 20. Also an analysis has been done which takes into account the arterial wall pressure at pre and post blockage sites shown in Fig. 21. The aim of this study is to detect a considerable change if any at these two sites which can be confirmed by externally measuring the pressure using very sensitive pressure sensors. A geometry of an artery of 60 mm length was created with 4 mm diameter. A Gaussian blockage was inserted with 0.01 mm interval and pressure across that blockage was found which is plotted in Fig. 22.

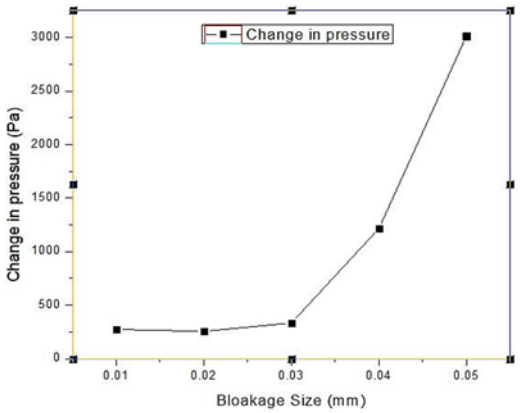

Fig. 22. Change in blood pressure at pre and post blockage site at varying blockage size.

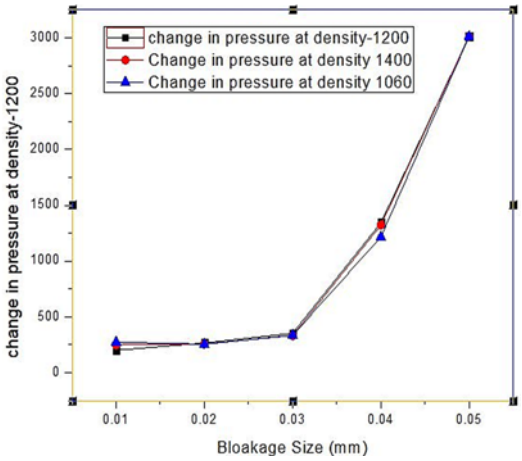

Fig. 23. Change in pressure at varying blood density and varying blockage size.

4. Conclusion

To detect the blockage in carotid artery by sensors externally an analytical model has been discussed which justifies that blockage can be detected of pressure difference between two points is maximum. Same can be done with velocity sensors, an abrupt increase in velocity at a point indicated blockage. Then two geometries has been discussed in this paper, first having a branch and its blockage its pressure and velocity profile has been discussed at pre an post blockage sites has been discussed.it was found that every blockage has its own fingerprint plot and its own behavior shown by their velocity an pressure profiles.it also reveals the condition when the pressure at those to sites become same. Then only plain carotid artery was taken into consideration and a graph was plotted at their post and pre blockage site whose difference was found to be exponentially increasing, the effect of varying blood density was not very comparable. These pressure and velocity profiles at different sites can be verified using MEMS pressure sensors and Doppler velocimeter. Hence this study gives the intuitive value of pressure at different points by which blockage and its type can be located.

References

[1]. Kasper D. L., Fauci A. S., Hauser S. L., Longo D. L. 1., Jameson J. L., Loscalzo J., Harrison's principles of internal medicine, 19th ed., *New York: McGraw Hill Education*, 2015.

[2]. B. Radic, Diagnosis and Treatment of Carotid Artery Stenosis, *J. Neurol. Stroke*, Vol. 7, Issue 3, 2017, pp. 9-12.
[3]. Salonen J. T., Salonen R., Ultrasonographically assessed carotid morphology and the risk of coronary heart disease, *Arterioscler. Thromb*, Vol. 11, 1991, pp. 1245-1249.
[4]. George J. Hademenos, Tarik F. Massoud, The physics of cerebrovascular diseases, *Springer*, New York, 1998.
[5]. M. Siebert, P. Fodor, Newtonian and Non-Newtonian Blood Flow over a Backward-Facing Step - A Case Study, in *Proceedings of the COMSOL Users Conference*, Boston, 2009.
[6]. J. Mazumdar, Biofluid Mechanics, *Singapore Ltd,* 1992.
[7]. Hall J. E. 1., Guyton and Hall textbook of medical physiology, 13th ed., Philadelphia, PA, *Elsevier*, 2016.
[8]. Jhalique Jane R. Foja, Rizalinda L. De Leon, Carotid Artery Modeling Using the Navier-Stokes Equations for an Incompressible, Newtonian and Axisymmetric Flow, *Elsevier*, 2013.
[9]. Agarwal R., Katiyar V. K., Pradhan P., A mathematical modeling of pulsatile flow in carotid artery bifurcation, *International Journal of Engineering Science,* Vol. 46, Issue 11, 2008, pp. 1147-1156.
[10]. Flori F., Giudicelli B., Di Martino B., A numerical method for a blood-artery interaction problem, *Mathematical and Computer Modelling*, Vol. 49, Issue 11-12, 2009, pp. 2145-2151.
[11]. P. Chuchard, *et al.,* Numerical simulation of blood flow through the system of coronary arteries with diseased left anterior descending, *International Journal of Mathematics and Computers in Simulation*, Vol. 5, Issue 4, 2011, pp. 334-341.
[12]. D. Espino, *et al.*, Simulation of blood flow through the mitral valve of the heart, A fluid structure interaction model, in *Proceedings of the COMSOL Users Conference,* Birminham, 2006.
[13]. J. Blazek, Computational fluid dynamics: Principles and applications, *Elsevier*, 2001.
[14]. Mancini G. B., Dahlof B., Diez J., Surrogate markers for cardiovascular disease: structural markers, *Circulation*, Vol. 109, 2004, pp. IV22–IV30.
[15]. A. Garje, Y. G. Adhav, D. Bodas, Design and Simulation of Blocked Blood Vessel for Early Detection of Heart Diseases, in *Proceedings of the 2nd International Symposium on Physics and Technology of Sensors*, Pune, India, 8-10 March 2015.
[16]. Malek A. M., Alper S. L., Izumo S., Hemodynamic shear stress and its role in atherosclerosis, *Journal of the American Medical Association*, Vol. 282, Issue 21, 1999, pp. 2035-2042.
[17]. Moosavi M., Fatouraee N., Katoozian H., Finite element analysis of blood flow characteristics in a ventricular assist device (VAD), *Simulation Modelling Practice and Theory*, Vol. 17, Issue 4, 2009, pp. 654-663.
[18]. Niroomand Oscuii H., Tafazzoli Shadpour M., Ghalichi F., Flow characteristics in elastic arteries using a fluid-structure interaction model, *American Journal of Applied Sciences,* Vol. 4, Issue 8, 2007, pp. 516-524.